Physics of Fluids

Numerical investigation of surface curvature effect on the self-propelled capability of coalesced drops

Cite as: Phys. Fluids **32**, 122117 (2020); https://doi.org/10.1063/5.0026163
Submitted: 21 August 2020 • Accepted: 10 November 2020 • Published Online: 18 December 2020

Yan Chen (陈燕), Ahmed Islam, Mark Sussman, et al.

Physics of Fluids ARTICLE scitation.org/journal/phf

Numerical investigation of surface curvature effect on the self-propelled capability of coalesced drops

Cite as: Phys. Fluids 32, 122117 (2020); doi: 10.1063/5.0026163
Submitted: 21 August 2020 • Accepted: 10 November 2020 •
Published Online: 18 December 2020

Yan Chen (陈燕),[1] Ahmed Islam,[1] Mark Sussman,[2] and Yongsheng Lian[1,a)]

AFFILIATIONS

[1] Mechanical Engineering Department, University of Louisville, Louisville, Kentucky 40223, USA
[2] Mathematics Department, Florida State University, Tallahassee, Florida 32306, USA

[a)] Author to whom correspondence should be addressed: yongsheng.lian@louisville.edu

ABSTRACT

We numerically investigate the curvature effect on the self-propelled capability of coalesced drops. The numerical method is based on a well validated multiphase flow solver that solves the three-dimensional Navier–Stokes equations. The liquid–air interface is captured using the moment of fluid method, and a direction splitting method is applied to advect the interface. Afterward, an approximate projection method is used to decouple the calculation of velocity and pressure. Different cases were validated by comparing the experimental results with the simulation results. The coalescence-induced jumping behavior on a flat surface is carefully captured using this numerical method. To investigate the effect of curvature of a curvy substrate on the self-jumping behavior, a case with a single drop impinging on a convex surface and a case with two drops' coalescence on a fiber are also studied and compared with the experimental results. The asymmetric bouncing of a single drop on the convex surface leads to 40% reduction in contact time, as found in our study. Our study also reveals that due to the curvature of the wedge, the drop forms a lobe shaped region on the symmetric sides of the wedge. The lobed region forces the drop to convert more surface energy into kinetic energy in the upward direction. The jumping capability is improved by increasing the surface curvature. Our study also shows that at lower angles of contact, the drops can easily get attached to the substrate and, at the same time, have difficulty detaching from the substrate.

I. INTRODUCTION

The self-propelled phenomenon has been discovered on various surfaces, from synthetic super-hydrophobic surfaces such as a lotus leaf to legs of a water strider.[1–3] The reason for the self-propelled phenomenon is due to the release of excess surface energy, which, therefore, converts into kinetic energy upon drop coalescence.[1–3] The self-propelled capability has drawn enormous attention[4–9] as it has played an important role in various engineering applications, such as heat exchangers,[10] anti-icing and anti-frost devices,[11–13] thermal management,[14,15] and water harvesting.[16,17]

Extensive research has been conducted to investigate the self-propelled behavior. Liu *et al.*[18] reported that the non-dimensional jumping velocity of ~0.2 of equally sized drops on Leidenfrost surfaces was observed to follow the capillary–inertial velocity and was consistent with that on superhydrophobic surfaces. Boreyko and Chen[1] confirmed the study Liu *et al.*[18] when they observed that the coalescence-induced velocity depends on the size of the drop, which, therefore, confirms the relation to the capillary–inertial velocity. Wang *et al.*[19] validated the capillary–inertial velocity with theoretical modeling where they showed that self-propelling behavior can only occur due to the surface energy, while the viscous dissipation and gravitational potential energy could be considered to have very negligible effect. Liu *et al.*[20] also found that the out of plane jumping is due to the non-wetting substrate interfering with the oscillation of the merged drop. From recent research studies, it is found that non-equal sized drops also jump out of the plane but at slower rebounding speed with much less useful translational kinetic energy compared to equal size drops.[21,22] Similarly, drops impacting on stationary drops on superhydrophobic surfaces can cause liquid bridging, which, in turn, produces reversed torque, causing the rebounding drop to have rotational motion.[23]

The water repellent capability of the lotus leaf and other natural surfaces has inspired numerous research studies of the superhydrophobic patterned surface.[24–28] The micro/nano-patterned surface shows very low adhesive force to water drops.[26,29–32] Therefore, the surface has a positive effect on the self-propelled jumping drops.[15,33] Wu *et al.*[28] found that the contact angle of a bent patterned surface increased from 150° to 160° and the adhesion force decreased significantly with a smaller curvature. Similarly, for impacting drops on wires with very small curvatures, the formation of lobe regions can cause the momentum transfer while storing enough inertia to lift the drop from the substrate.[34,35]

The curved surface was found to have a positive effect on the performance of the bouncing liquid.[36] Hao *et al.*[36] investigated the bouncing capability of a water drop on a flat thin oil film. The bouncing phenomenon occurred only on a spherical surface but not on the other two surfaces with different arrays. Liu *et al.*[37] found the contact time of a bouncing drop on a curved surface to be 30% shorter than that on an equivalent flat surface.[38–40] A faster asymmetric bouncing phenomenon due to the curved surface is observed in both experimental and simulation based studies.[37] Zhang *et al.*[41] studied the self-propelled behavior on fiber-based coalescers and claimed that the curvature of the fiber played a critical role in the self-bouncing capability of the drops upon coalescence. The self-bouncing process upon drop coalescence occurred on a fiber at contact angles of $\theta_A/\theta_R = 120°/110°$ (where θ_A and θ_R are the advancing and receding contact angles, respectively). The effect of the curved surface was believed to accelerate the merged drop orthogonal to the fiber and obey the capillary–inertial law.[18,20] Unlike the flat surface, the fiber had less solid to liquid area of contact, reducing the substrate–drop adhesion. The early intervention to the coalescence effectively harnessed the released energy toward useful translational motion.

In the present study, we numerically investigate the drop coalescence-induced jumping phenomena on curved wedges having different degrees of curvature. This paper is structured as follows. At first, we briefly describe the numerical method we used to solve the problem. Second, we validate our code by comparing experimental results with the simulation results. Subsequently, we investigate the drop impact on the curved surface compared to the flat surface and drop coalescence and jumping phenomena on surfaces with different curvatures. Finally, we study the effect of surface adhesion on a curved wedge.

Different models have been used to analyze the jumping capability.[5,18,42] The theoretical jumping velocity can be obtained when supposing all excessive surface energy is converted into kinetic energy in the jumping direction, and therefore, an empirical model is obtained based on the experimental data.[5,18,42] While detailed derivation is presented in our previous study,[43] we briefly present the theoretical analysis of drop jumping phenomena using the theoretical jumping velocity defined as

$$w_j = \sqrt{\frac{\sigma}{\rho_l r_0}}, \tag{1}$$

where w_j is the jumping velocity, σ is the surface tension, ρ_l is the drop density, and r_0 is the drop radius.

Upon drop coalescence, the release of excessive surface energy can be explained using a simple model shown in Fig. 1.

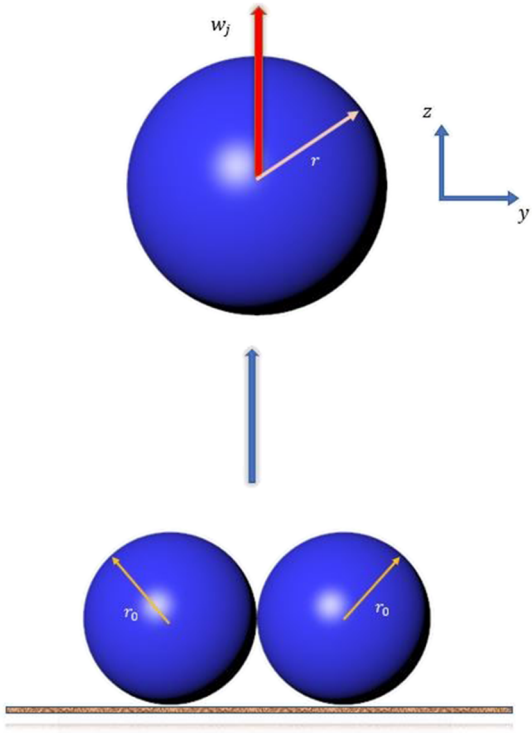

FIG. 1. Schematic of the drop coalescence process on a non-wetting substrate.

The merged drop has a mass of

$$m = \frac{8}{3}\rho_l \pi r_0^3. \tag{2}$$

Then, the kinetic energy of the merged drop could be defined as follows:

$$E_k = \frac{1}{2}m(u^2 + v^2 + w^2). \tag{3}$$

During coalescence, the energy within the system undergoes continuous conversion from one form to another, namely, within surface energy, kinetic energy, potential energy, and viscous dissipation energy. The change in the potential energy is neglected, and the surface energy of a stationary drop on a hydrophobic surface can be written as

$$E_s = \sigma_{lv}A_{lv} + \sigma_{ls}A_{ls} + \sigma_{sv}A_{sv}, \tag{4}$$

where A is the interfacial area, σ is the surface tension, and the subscripts s, l, and v denote the solid, liquid, and vapor, respectively.

Because the overall surface area is reduced upon coalescence, excessive surface energy is released. The released surface energy could be written as $\Delta E_s = 4\sigma\pi r_0^2(2 - 2^{2/3})$, and the released surface energy converts into kinetic energy, which helps the merged drop to jump and accelerate away from the plane substrate.[1,18,41,43]

Empirical models[18,44] were obtained from different experiments.[1,18,44] Liu *et al.*[18] studied the coalescence-induced jumping phenomena on flat surfaces with drop sizes ranging from 20 μm to 500 μm. Enright *et al.*[44] also obtained a jumping velocity model from

both their experimental data and Boreyko and Chen's[1] data. They proposed the following model to predict jumping velocity:

$$w_j = Du_{ci}, \tag{5}$$

where parameter D is a function of the Ohnesorge number, Oh,

$$D = 3.4026Oh^2 - 1.5285Oh + 0.2831, \tag{6}$$

$$Oh = \frac{\mu}{\sqrt{\rho_l \sigma D_0}}, \tag{7}$$

where D_0 is the diameter of the drop. In addition to the Ohnesorge number, Oh, we would also report the Weber numbers in our study, defined as follows:

$$We = \frac{\rho_l U_0 D_0}{\gamma}. \tag{8}$$

Derived from the capillary–inertia velocity, the corresponding characteristic timescale is given as

$$\tau_j = \frac{r_0}{u_{ci}} = \sqrt{\frac{\rho_l r_0^3}{\sigma}} \tag{9}$$

and is used to non-dimensionalize the simulation time of this study. In addition to time, velocity, momentum, and kinetic energy are also non-dimensionalized by the characteristic relationships, as shown below.

For time,

$$t^* = t/\tau_j = \frac{t}{\sqrt{\rho_l r_0^3/\sigma}}. \tag{10}$$

For velocity,

$$v^* = \frac{v}{u_{ci}}. \tag{11}$$

For momentum,

$$p^* = \frac{p}{\rho_l(\frac{8}{3}\pi r_0^3)u_{ci}}. \tag{12}$$

For energy,

$$E_z{}^* = \frac{KE_z}{\rho_l(\frac{8}{3}\pi r_0^3)u_{ci}^2}. \tag{13}$$

For the characterization of the kinetic energy in the drop bouncing and the drop coalescence process, we used the overall kinetic energy in the z-direction from the drop (liquid phase) in the computation domain. It is because after drop impact–bounce and drop coalescence-induced jumping from the curved wedges, the traveling drops would be constantly oscillating from an oblate to a prolate shape, and vice versa, and the integrated scalar value over the whole domain does not correctly take into account the overall trajectory of the drop in motion and produces an alternating kinetic energy. Hence, it is ideal to use the drop as a point mass as it travels in a defined direction (which, in our case, is the z-direction), to deduce the following momentum and kinetic energy equations:

$$P_z = mv_z, \tag{14}$$

$$KE_z = \frac{1}{2}mv_z^2. \tag{15}$$

II. NUMERICAL METHOD

We will briefly discuss the important steps in our numerical method here. The detailed description of the numerical method can be found in the earlier papers.[43,45–47]

A. Governing equations

The governing equations for incompressible, immiscible, multiphase flows are given as

$$\nabla \cdot u = 0, \tag{16}$$

$$\frac{\partial u}{\partial t} + u \cdot \nabla u = -\frac{\nabla p}{\rho} + \nabla \cdot \frac{2\mu D}{\rho} + g - \frac{1}{\rho}\sum_{m-1}^{M} \gamma_m \kappa_m \nabla H(\phi_m), \tag{17}$$

where $\boldsymbol{u} = (u, v, w)$ is the velocity vector, t is the time, p is the pressure, $\boldsymbol{g}$ is the gravitational acceleration vector, D is the rate of deformation tensor, and ρ and μ are the density and viscosity for the material m, ∇H being the Heaviside step functions of the Level-Set (LS) function, ϕ_m. The stress at the material interface (m_1 and m_2 being two different materials) follows the jump condition

$$((-p_{m_1} I + 2\mu_{m_1} D) - (-p_{m_2} I + 2\mu_{m_2} D)) \cdot \boldsymbol{n}_{m_1} = \sigma_{m_1,m_2}\kappa_{m_1}\boldsymbol{n}_{m_1}, \tag{18}$$

where σ_{m_1,m_2} is the surface tension coefficient, $\boldsymbol{n}_{m1}$ is the normal pointing from material m_2 into m_1,

$$\boldsymbol{n}_{m1} = \frac{\nabla\phi_{m1}}{|\nabla\phi_{m1}|}, \tag{19}$$

and κ_{m_1} is the curvature,

$$\kappa_{m_1} = \nabla \cdot n_{m_1}. \tag{20}$$

In order to reconstruct the correct fluid interface, the moment of fluid (MOF) interface reconstruction algorithm is used at the interfaces between different phases. Even though the MOF method can be considered a generalized model of volume-of-fluid (VOF) method, the MOF method relies on information solely from the cell under consideration, and in addition to the volume information (zeroth-order moment), it also uses the centroid information (first-order moment) of the cell under consideration,

$$F_m = \frac{1}{|\Omega_{i,j}|}\int_{\Omega_{i,j}} H(\phi_m(\boldsymbol{x}))d\boldsymbol{x}, \tag{21}$$

$$\boldsymbol{x}_m = \frac{\int H(\phi_m(\boldsymbol{x}))\boldsymbol{x}d\boldsymbol{x}}{\int_{x_{i-1/2}}^{x_{i+1/2}}\int_{y_{j-1/2}}^{y_{j+1/2}} H(\phi_m(\boldsymbol{x}))x}. \tag{22}$$

Using piecewise linear interface construction (PLIC), the interface reconstruction procedure minimizes the following interface equation:

$$\boldsymbol{n} \cdot (\boldsymbol{x} - \boldsymbol{x}_{i,j}) + b = 0, \tag{23}$$

using the following constraints:

$$|F_{ref} - F_{act}| = 0, \tag{24}$$

$$E_{MOF} = ||\boldsymbol{x}_{ref}^c - \boldsymbol{x}_{act}^c||^2, \tag{25}$$

where F_{ref} and x_{ref} are the referenced volume fraction and centroid location and F_{act} and x_{act} are the reconstructed volume fraction

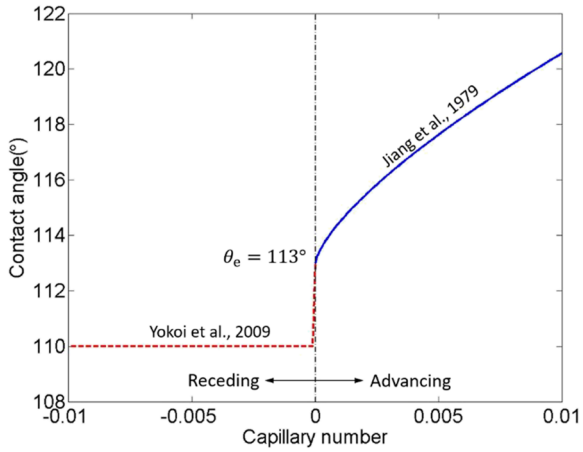

FIG. 2. Dynamic contact angle vs capillary number.

and centroid location. Constraining the optimization problem helps achieve an accurate, reconstructed interface at the boundary of two or more different materials/phases. For more detailed discussion on the moment of fluid (MOF) reconstruction method, other literature including studies by Li *et al.*[47] and Ahn *et al.*[48–52] should be referred.

B. Dynamic contact angle models

In this paper, the dynamic contact angle is applied to model the contact line as a boundary condition. The model of Jiang *et al.*[53] is used in this study, and the value of the contact angle depends on the capillary number. Jiang's model is derived from the experimental measurement by Hoffman.[54] Since the model of Jiang *et al.* is valid only for the advancing contact angle, Yokoi's model I[55] is used for the receding motion where a constant minimum receding contact angle is obtained from the experimental measurement,[41]

$$\cos\theta_m = \begin{cases} \cos\theta - (\cos\theta_s + 1)\tanh(4.96Ca^{0.702}), & Ca \geq 0 \\ \cos\theta_r, & Ca < 0, \end{cases} \quad (26)$$

where θ_m is the dynamic contact angle, θ_s is the static contact angle, and θ_r is the receding angle. The dynamic contact angle model is shown in Fig. 2.

TABLE I. Water properties at 20 °C or 100 °C.

	σ (mN m^{-1})	μ_l (mPa s)	μ_g (mPa s)	ρ_l (kg m^{-3})	ρ_g (kg m^{-3})
20 °C	72.7	1.071	0.0182	998	1.190
100 °C	58.9	0.282	0.0219	958	0.934

III. RESULTS AND DISCUSSIONS

We first validate the code by comparing simulation results with the experimental results from two different cases. Afterward, we investigate the drop impact and bouncing phenomena on a curved substrate and a flat substrate. Then, we investigate the effects of curvature by simulating the drop coalescence on single-stripe patterned surfaces. The curvatures of wedges on the surfaces vary, while the contact angle remains constant at 180°. The effect of contact angles on coalescence-induced jumping is investigated by varying the contact angles.

A. Code validation

1. Case validation I

For the first case validation, we employ our previous study[43] of water drop coalescence on a substrate at a contact angle of 180°. The drops having a diameter of 380 μm and fluid properties at T = 100 °C, as shown in Table I, were used to validate the simulation results with the experimental results from the study of Liu *et al.*[18] Detailed simulation settings and grid sensitivity analysis are also described in the previous study.[43] The simulation showed good match with the experimental results and was able to capture the drop deformation shapes during the entire process of coalescence. The jumping behavior is also captured in the simulation, and the predicted jumping speed of 0.09 m/s is very close to the experimental result of 0.08 m/s.

2. Case validation II

In the second case, we validate the code for the coalescence-induced self-bouncing phenomenon on a fiber at advancing and receding contact angles of 120° and 110°, respectively. The radius of the water drop is 249 μm, and the radius of the fiber is 46 μm. The water properties at 20 °C in Table I are used. Figure 3 compares the experimental (a) and numerical (b) results during the self-bouncing

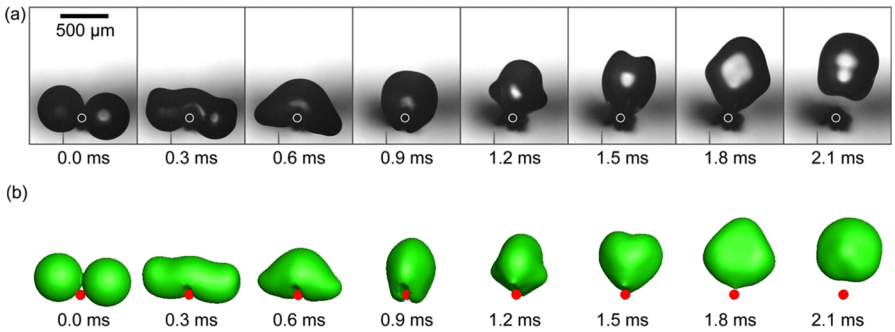

FIG. 3. Comparison of experimental[41] (a) and simulation (b) results of self-bouncing behavior on a fiber.

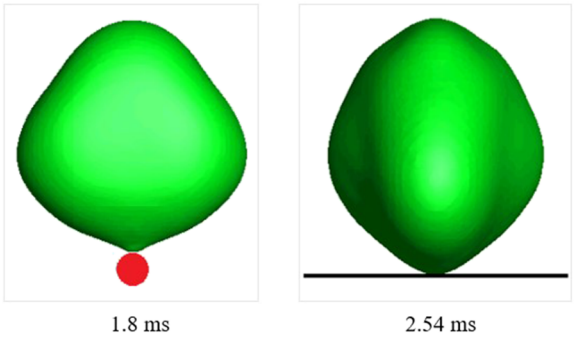

FIG. 4. Drop detachment instance: fiber vs flat surface.

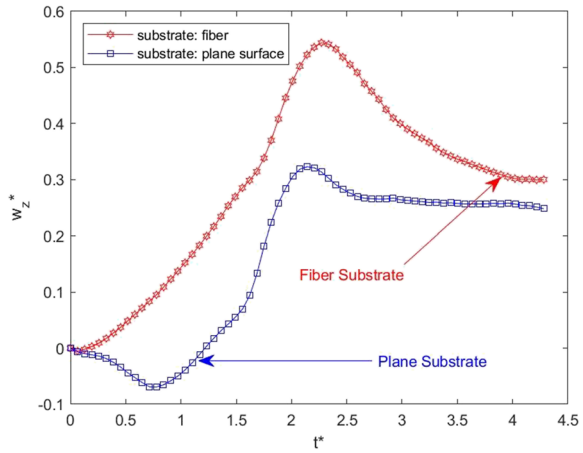

FIG. 5. Comparison of the normalized jumping speed of the coalesced drops on two different substrates, fiber and plane surface.

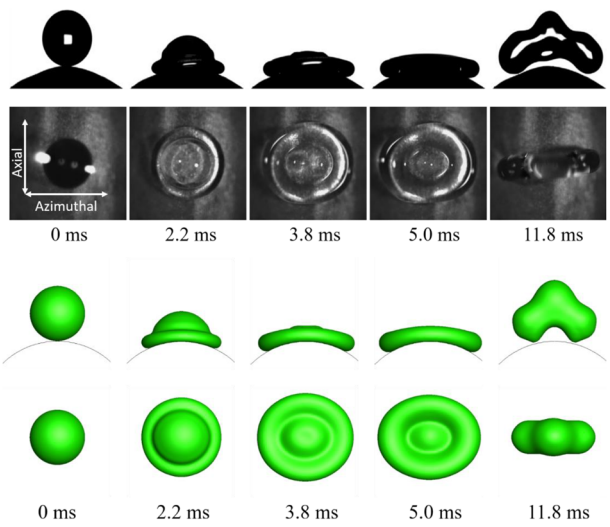

FIG. 6. Comparison of experimental results[37] (top) and simulation results (bottom) of a single drop bouncing off from the curved surface.

process on the fiber. The two drops coalesce into a single drop that subsequently deforms and detaches from the fiber. The simulation correctly captures the drop deformation and bouncing behavior on the fiber.

To understand the effect of fiber during the coalescence process and the subsequent jumping phenomenon, the case of coalescence on a fiber is being compared to the case of coalescence on a flat substrate. The coalesced droplet on a fiber has shown much earlier detachment ($T_{Fiber\text{-}Detachment}$ = 1.8 ms) compared to that on the flat surface ($T_{Flat\text{-}Detachment}$ = 2.54 ms), as shown in Fig. 4.

The jumping speed is analyzed. Here, we consider the coalesced droplet as a point mass. As shown in Fig. 5, it is evident that there is higher jumping speed in the case of the fiber substrate compared to that of the flat surface. In the case of jumping on the fiber substrate, the maximum trajectory speed of $w^*_{z\_Fiber}$ = 0.546 is 68% higher than the trajectory speed of $w^*_{z\_Flat}$ = 0.32 on a flat substrate.

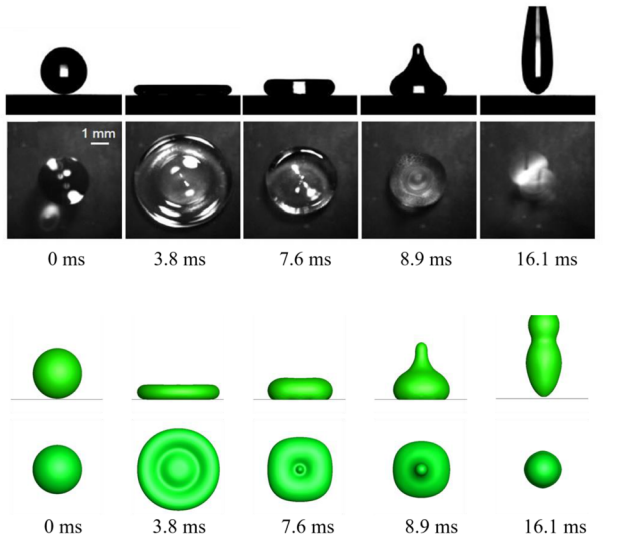

FIG. 7. Comparison of experimental results[37] (top) and simulation results (bottom) of a single drop bouncing off from the flat surface.

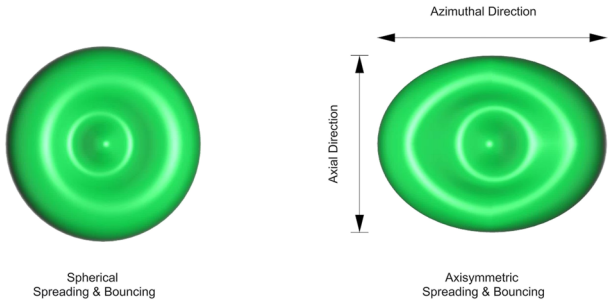

FIG. 8. Characteristic of spherical vs asymmetric spreading and bouncing.

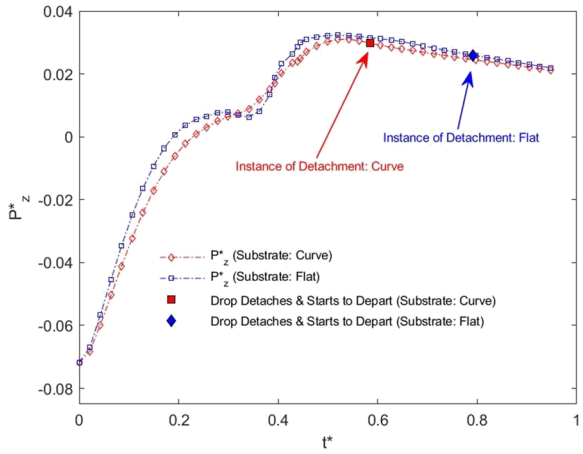

FIG. 9. Comparison of momentum data of a single drop bouncing off from the curved and flat surfaces.

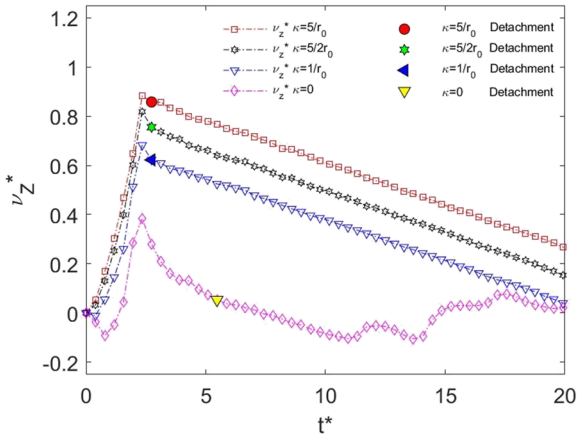

FIG. 11. Comparison of the z-axis velocity on different curvature surfaces during the drop jumping process.

B. Drop impact on a curve surface

To understand the effect of substrate curvature on self-jumping behavior, we compare our simulation results with the experimental results obtained by Liu *et al.*[37] for a drop impinging on the convex surface of *Echeveria* leaf. The same drop bouncing was conducted on a flat surface for comparison. A liquid water drop having a diameter of 2.9 mm at 20 °C is used in this case, and the diameter of the convex surface is set at 8.2 mm. The impact velocity of the drop is 0.63 m/s corresponding to the Weber number We = 7.9 and Ohnesorge number Oh = 0.0028. The contact angle is 160°.

The experimental and numerical results of the drop bouncing process on curved surfaces are compared in Fig. 6. Then, the comparison to the flat surface is shown in Fig. 7. The simulation shows good agreement with the experimental results. It correctly predicts the shape of the deformed drop and captures the moment the drop bounces off from the curved surface. An asymmetric bouncing, as described in the literature by Liu *et al.*,[37] where the droplet spreads more in the azimuthal direction than in the axial direction, as seen in Fig. 8, is captured on a convex surface, and the contact time is 40% less than that on a flat surface. The drop undergoes fast retraction in the axial direction, resulting in an uneven distribution of momentum and mass between the axial direction and the azimuthal direction. The asymmetric bouncing simulation confirmed the physics believed to enable the drop have less contact time on the convex surface than on the flat surface.[37]

The advantage of asymmetric bouncing is shown in Fig. 9. It is clearly seen that the drop on a curved surface departs much earlier and has much less contact time than the drop on the flat surface.

There is a great deal of interest for this reduced contact time and early departure, since faster and enhanced water repellency could benefit in heat transfer and anti-icing.[1,37,56,57] Similarly, according to microbiology and medical science research, faster detachment could mean less time for viral and bacterial disposition, since it is known that drops could actively participate in transmitting pathogens and diseases.[37,58,59]

C. Drop coalescence-induced jumping on a wedge curvature

To study the effect of curvature on the jumping behavior upon drop coalescence, a wedge is placed on the flat surface. In this study, we systematically vary the wedge curvature. Our study reveals that with an increase in the curvature of the wedge, the jumping capability of the coalesced drop also increases. For each of the simulations, the radii of the water drops are set to 380 μm and the properties of liquid and air at 100 °C, as shown in Table I, are used. The contact angle to the surface is set to 180°, and therefore, the surface adhesion does not exist during the simulation. Case validation I is considered a case for comparison, and the curvature of the wedge is set at $\kappa = 0$. The beginning status of drop coalescence on different wedges is shown in Fig. 10. The drops coalesce along the horizontal, i.e.,

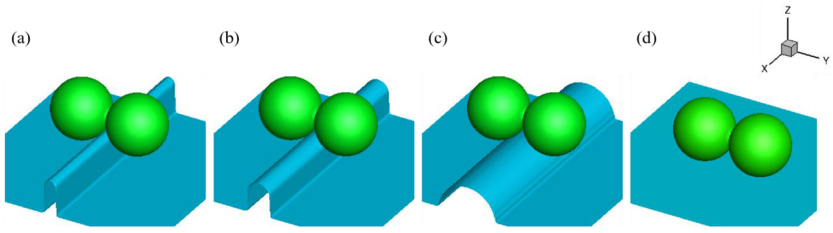

FIG. 10. Computational domains of substrate surfaces with different curvatures: (a) $\kappa = 5/r_0$; (b) $\kappa = 5/(2r_0)$; (c) $\kappa = 1/r_0$; (d) $\kappa = 0$ (flat surface).

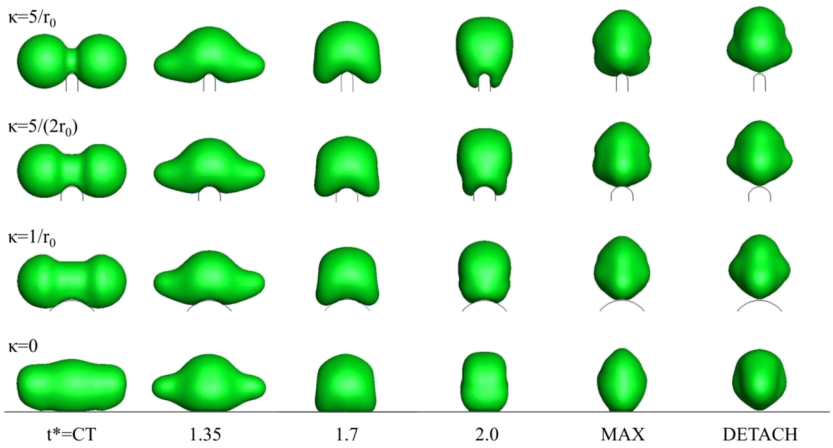

FIG. 12. Drop coalescence process on the surface (θ = 180°) with different curvatures (y–z plane).

y-axis, direction, and the self-propelled behavior occurs in the vertical or z-axis direction. In Figs. 10(a)–10(c), the y-axis radii of the wedges are $0.2r_0$, $0.4r_0$, and r_0, and the curvatures are $\kappa = 5/r_0$, $\kappa = 5/(2r_0)$, and $\kappa = 1/r_0$, respectively.

The z-axis velocity of the four cases during the coalescence processes is plotted in Fig. 11. Overall, the cases with the wedges have enabled jumping drops with higher z-axis velocities than those in the case with the flat surface. The jumping speed at the moment of detachment increases with the increase in curvature. The drop on the wedge with larger curvatures accelerates earlier in the positive z-axis direction. The instance of detachment is mostly delayed by substrates with larger curvatures and is found to be most delayed with the flat substrate.

To investigate the differences in the z-axis velocity, we compare the shapes of coalesced drops from the views of the y–z plane in Fig. 12. When two drops start to coalesce, a liquid bridge forms, as depicted in $t^* = CT$. The formation of this liquid bridge consequently forms a close contact with the wedge substrate. From our simulation, it is evident that a larger curvature leads to an earlier contact of the liquid bridge with the substrate.

For the next frames, we plot three other time instances before the instances of detachment: $t^* = 1.35$, $t^* = 1.7$, and $t^* = 2.0$. At $t^* = 1.7$, the fluid starts forming a small lobed region at the bottom of the drop near the wedge. At $t^* = 2.0$, the small lobe connects the wedge with the maximum contact area, as shown in Fig. 13. The concentrated area of small lobe increases with the increase in the substrate curvature.

The pressure difference due to Laplace pressure[60] between a gas region and a liquid region can be explained as $\Delta p = 2\gamma/R_c$, where γ is the surface tension and R_c is the radius of the gas–liquid interface. The lobe area of the drop in the case of a larger curvature has a higher pressure difference. The larger curvature also causes a delay in the occurrence of the maximum z-axis speed. The evolving shape transformation during the drop coalescence-induced jumping shows that the small lobe region acts as a trajectory for the jumping drops. The shape of the lobe region, giving a spring motion for the jumping drops, is dependent on the substrate underneath. From $t^* = 2.0$ until the moment of drop detachment, the rate at which the detachment from the surface area occurs in the case of a curved wedge is more than that in the case of the flat surface. As observed in Fig. 12, the small lobes on the wedge surface start to disappear ($t^* > 2.0$), resulting in the release of surface energy residing in those

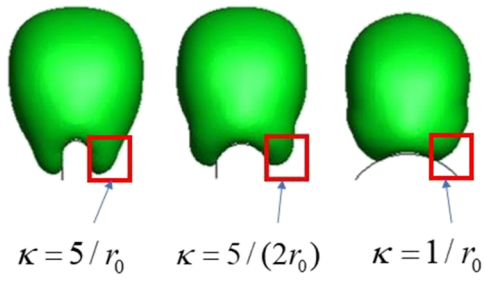

FIG. 13. Lobe formation around different wedge curvatures, $t^* = 2.0$.

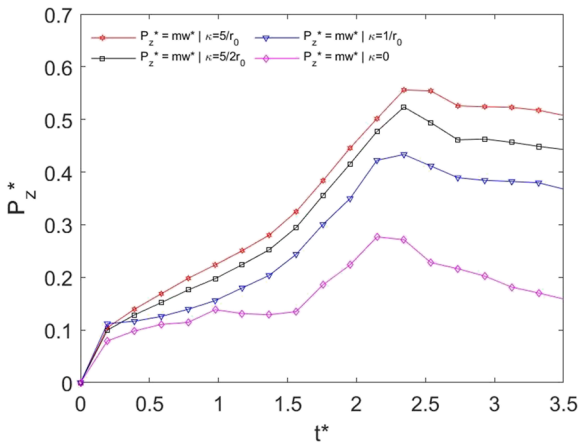

FIG. 14. Momentum ratio in the z-direction for the first $t^* = 3.5$ shown for drop jumping with different curvatures.

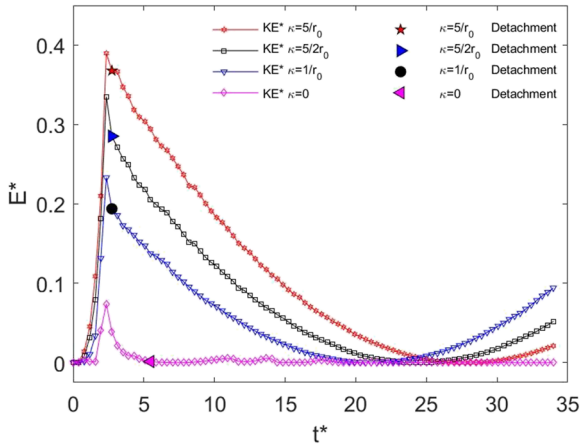

FIG. 15. Comparison of the dimensionless kinetic energy over time during the self-propelled process for the cases with $\kappa = 5/r_0$, $\kappa = 5/(2r_0)$, $\kappa = 1/r_0$, and $\kappa = 0$.

regions. The surface energy is converted into kinetic energy, and this rate of transformation becomes more prominent as the degree of curvature increases. Figure 14 confirms the striking difference in non-dimensional momentum, which is due to the underlying substrate curvature, and that the curvature of $\kappa = 5/r_0$ exhibits almost double the maximum momentum ratio $\max P_z^* = 0.56$ compared to that of the flat substrate $\max P_z^* = 0.25$.

In Fig. 15, the flat surface has the lowest kinetic energy in the z-axis direction and the magnitude of kinetic energy is higher on the wedge with a larger curvature. In addition, the coalesced drop detaches from the wedge substrates much earlier than from the flat

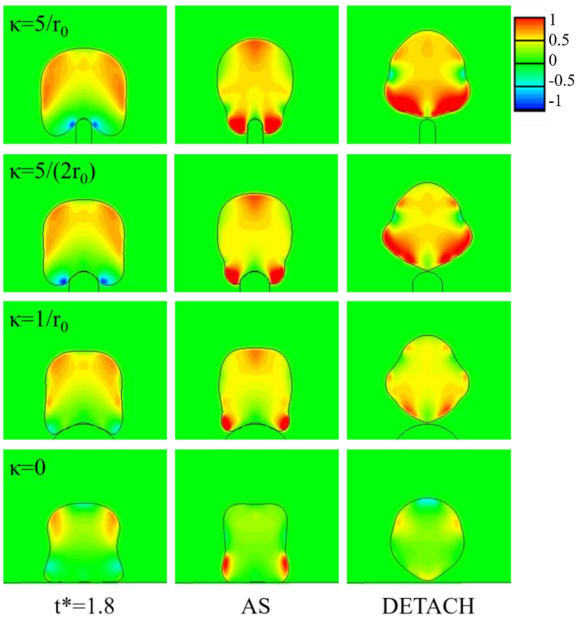

FIG. 16. z-axis velocity contours on the surfaces with different curvatures.

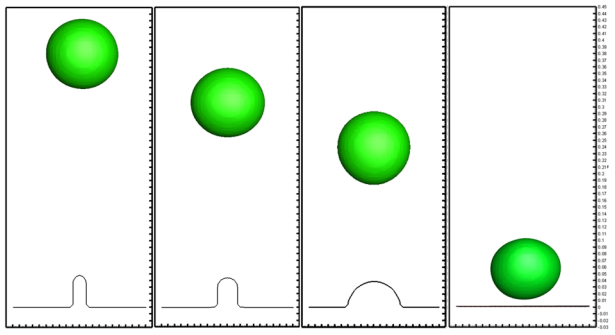

FIG. 17. Final droplet height achieved with different curvatures, $\kappa = 5/r_0$, $\kappa = 5/(2r_0)$, $\kappa = 1/r_0$, and $\kappa = 0$.

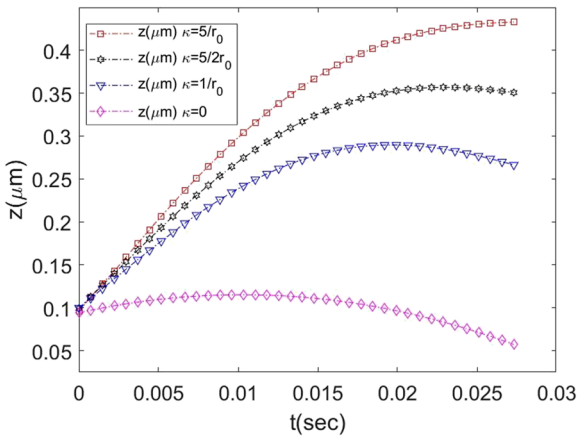

FIG. 18. Drops traveling in the z-axis direction due to coalescence on substrates with different curvatures ($\kappa = 5/r_0$, $\kappa = 5/(2r_0)$, and $\kappa = 1/r_0$).

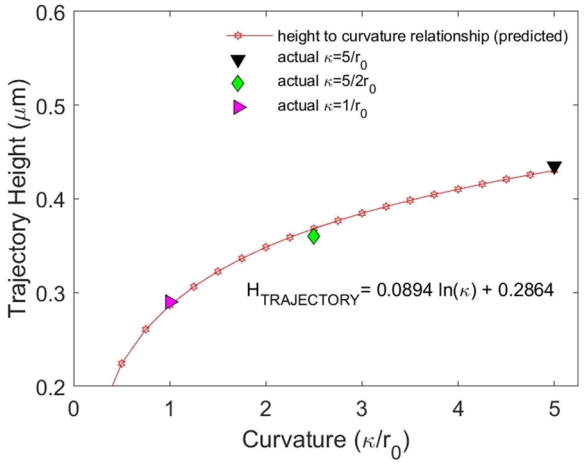

FIG. 19. Relationship between the achievable trajectory height and the curvature of the wedged substrate.

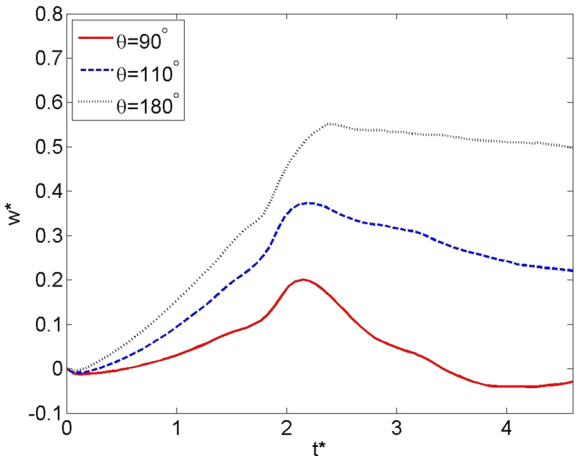

FIG. 20. Comparison of the z-axis velocity on the surfaces with the same curvature of $\kappa = 5/r_0$ but different contact angles during the drop jumping process.

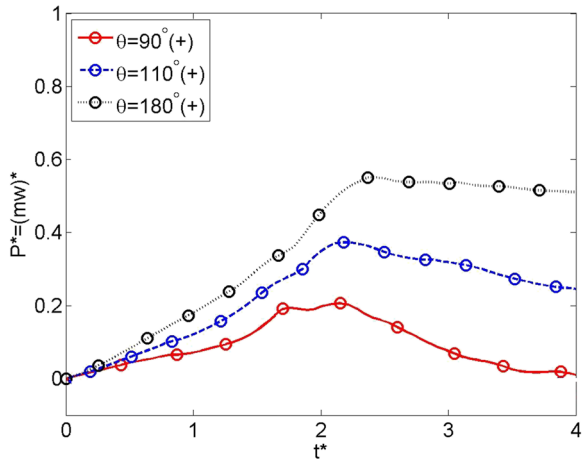

FIG. 21. Comparison of z-axis momentums on the surfaces with the same curvature of $\kappa = 5/r_0$ but different contact angles during the drop jumping process.

surface, confirming a similar characteristic of enhanced capability of drop detachment during the impact and bounce of a single drop discussed earlier (Fig. 16).

To investigate how the jumping motion changes over time, the z-axis velocity contours are plotted on the y–z plane at three time instants: (1) $t^* = 1.8$, (2) the moment of maximum surface area contact by the spread of the lobe region, and (3) the moment at which drop detachment occurs. In conjunction with Fig. 12, it is clear that a larger curvature leads to a higher velocity, which is further evident in the velocity contours shown above. At $t^* = 1.8$, the negative z-axis velocity appears on the contour plot at the bottom of the drop. Later, the positive velocity appears near the bottom of the drop due to the pressure difference resulting from the large curvature area of the lobe region. The drop starts to accelerate at the bottom, and the time instants for the four cases are 2.2, 2.05, 2.0, and 2.0, respectively. At the instance of drop detachment, the upward velocity near the wedge is higher when the curvature is larger.

The kinetic energy plot, along with the velocity contour plots for the examined surfaces, indicates that the drop coalescence-induced jumping phenomena can be greatly enhanced with the increase in the substrate surface curvature.

The final height achieved through our investigation of different substrates shows the clear advantage of having substrate curvatures. The wedge curvature enables the coalescing drops to come into less contact with the substrate. Figures 17 and 18 show that $\kappa = 5/r_0$ achieves a maximum height of $h_z = 0.435\ \mu$m, followed by $\kappa = 5/(2r_0)$ reaching $h_z = 0.360\ \mu$m and $\kappa = 1/r_0$ reaching $h_z = 0.290\ \mu$m.

With the increase in curvature, the coalesced drop can stay suspended in the air for a longer period of time, with $\kappa = 5/r_0$, $\kappa = 5/(2r_0)$, and $\kappa = 1/r_0$ taking 27.3 ms, 24.4 ms, and 21.03 ms, respectively, to reach the maximum height. The evidence of the curvature substrate enhancing the final jumping height is prominent when compared to the flat substrate $\kappa = 0$, which could only achieve a jumping height of $h_z = 0.1025\ \mu$m and much shorter traveling time of 7.74 ms to reach the maximum height.

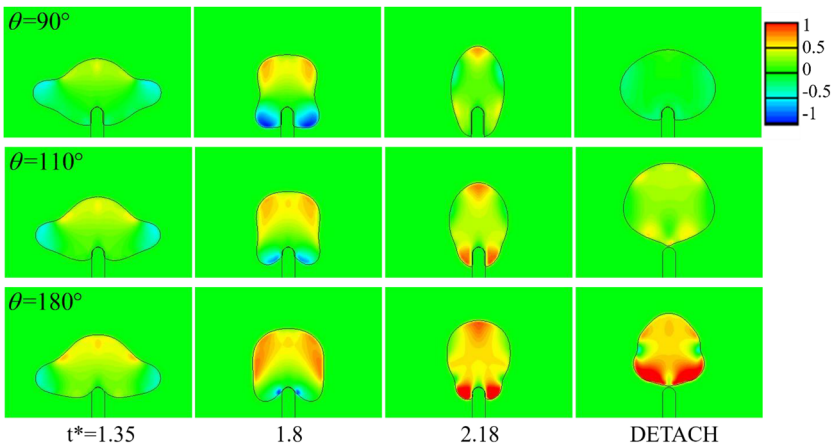

FIG. 22. Dimensionless z-axis velocity contours on the surfaces with the same curvature of $\kappa = 5/r_0$ but different contact angles.

We propose the following correlation between the surface curvature and the achievable jumping height based on our findings:

$$H_{TRAJECTORY} = 0.0894\ln(\kappa) + 0.2864. \quad (27)$$

Figure 19 shows the correlation.

D. Surface adhesion effect on the wedged surfaces ($\kappa = 5/r_0$)

To understand the effect of surface adhesion, we simulate drop self-jumping on surfaces with the same curvature ($\kappa = 5/r_0$) but different contact angles (90°, 110°, and 180°). Our simulation shows that the drop on a surface at a contact angle of 90° lacks self-propelling capability. The dimensionless z-axis velocity profile is plotted in Fig. 20 and shows that the z-axis velocity increases with the angle of contact during the whole coalescence process. The momentums in the positive z-axis direction are plotted in Fig. 21. It can be seen that a higher contact angle leads to a higher momentum in the z-direction.

The contour plots of the z-axis velocity at different contact angles are plotted in Fig. 22. The drop with a contact angle of $\theta = 90°$ has more lobe region attachment with the substrate (a higher magnitude of the substrate–droplet contact). At $t^* = 1.8$, the case of $\theta = 90°$ shows a higher velocity in the negative z-axis direction. At $t^* = 2.18$, a higher velocity in the positive z-axis is observed for the 180° contact angle case. The detaching moment of $\theta = 110°$ and $\theta = 180°$ is $t^* = 4.07$ and $t^* = 2.56$, respectively. The detaching velocity is much higher on the surface of $\theta = 180°$. The drop of $\theta = 90°$ is unable to detach from the substrate.

IV. CONCLUSIONS

Numerical simulations were conducted to investigate the curvature effect on the self-propelled behavior during drop coalescence. The Navier–Stokes equations were solved using the projection method on Cartesian grids, and the moment of fluid method was used to capture the interfaces. The code was validated first by comparing the numerical results with the experimental results, and good agreement was achieved. The curvature effect was investigated by varying the curvatures. The adhesion effect was also studied.

The following important conclusions can be made from the present study: (i) Substrates with curvature allow impact and bouncing drops to detach faster compared to flat substrates. There is 40% less contact time of the drop to the substrate for the curved surface than the flat surface. (ii) The curvature of the substrate surface also affects the coalescence-induced drop jumping velocity and trajectory height. On the curved wedge, the drops contact the substrate earlier, preventing the development of negative jumping speed at an earlier stage. The coalesced drops form a lobe-shaped area near the curved wedge, and this region is smoothed out in the later stage releasing more surface energy and accelerating the drop in the jumping direction. The jumping velocity increases with the increase in curvature. Due to a higher jumping velocity, the drops' trajectory height also increases significantly. (iii) The adhesion of the substrate affects the self-propelled behavior on the substrate during the whole coalescence process. More negative jumping velocity is formed within the lobe region releasing the surface energy at higher contact angles. The adhesion, thus affects the amount of kinetic energy released to help the jumping process.

Our study revealed the curvature effect of the surface on the drop bounce and self-propelled behavior. The curved surface changes the deforming shape of the drops and has a positive effect on accelerating the jumping velocity by converting more surface energy to kinetic energy and transferring into the jumping direction. The substrate adhesion also changes the deforming shape of drops and generates more negative jumping velocity. The adhesion prevents the drop from releasing surface energy, and more energy is consumed by the adhesion.

ACKNOWLEDGMENTS

This research was partially supported by the NSF (Grant No. 1916114).

DATA AVAILABILITY

The data that support the findings of this study are available from the corresponding author upon reasonable request.

REFERENCES

[1] J. B. Boreyko and C.-H. Chen, "Self-propelled dropwise condensate on superhydrophobic surfaces," Phys. Rev. Lett. **103**, 184501 (2009).
[2] C. Lv, P. Hao, Z. Yao, Y. Song, X. Zhang, and F. He, "Condensation and jumping relay of droplets on lotus leaf," Appl. Phys. Lett. **103**, 021601 (2013).
[3] Q. Wang, X. Yao, H. Liu, D. Quéré, and L. Jiang, "Self-removal of condensed water on the legs of water striders," Proc. Natl. Acad. Sci. U. S. A. **112**, 9247 (2015).
[4] J. B. Boreyko and C. P. Collier, "Delayed frost growth on jumping-drop superhydrophobic surfaces," ACS Nano **7**, 1618 (2013).
[5] R. Enright, N. Miljkovic, N. Dou, Y. Nam, and E. N. Wang, "Condensation on superhydrophobic copper oxide nanostructures," J. Heat Transfer **135**, 091304 (2013).
[6] N. Miljkovic, R. Enright, Y. Nam, K. Lopez, N. Dou, J. Sack, and E. N. Wang, "Jumping-droplet-enhanced condensation on scalable superhydrophobic nanostructured surfaces," Nano Lett. **13**, 179 (2012).
[7] N. Miljkovic, R. Enright, and E. N. Wang, "Effect of droplet morphology on growth dynamics and heat transfer during condensation on superhydrophobic nanostructured surfaces," ACS Nano **6**, 1776 (2012).
[8] Y. Shi, G. H. Tang, and H. H. Xia, "Investigation of coalescence-induced droplet jumping on superhydrophobic surfaces and liquid condensate adhesion on slit and plain fins," Int. J. Heat Mass Transfer **88**, 445 (2015).
[9] D. Torresin, M. K. Tiwari, D. Del Col, and D. Poulikakos, "Flow condensation on copper-based nanotextured superhydrophobic surfaces," Langmuir **29**, 840 (2013).
[10] D. Reay, R. McGlen, and P. Kew, *Heat Pipes: Theory, Design and Applications* (Butterworth-Heinemann, 2013).
[11] J. B. Boreyko, R. R. Hansen, K. R. Murphy, S. Nath, S. T. Retterer, and C. P. Collier, "Controlling condensation and frost growth with chemical micropatterns," Sci. Rep. **6**, 19131 (2016).
[12] Q. Zhang, M. He, J. Chen, J. Wang, Y. Song, and L. Jiang, "Anti-icing surfaces based on enhanced self-propelled jumping of condensed water microdroplets," Chem. Commun. **49**, 4516 (2013).
[13] Q. Zhang, M. He, X. Zeng, K. Li, D. Cui, J. Chen, J. Wang, Y. Song, and L. Jiang, "Condensation mode determines the freezing of condensed water on solid surfaces," Soft Matter **8**, 8285 (2012).
[14] J. B. Boreyko and C.-H. Chen, "Vapor chambers with jumping-drop liquid return from superhydrophobic condensers," Int. J. Heat Mass Transfer **61**, 409 (2013).

[15]C. Dietz, K. Rykaczewski, A. G. Fedorov, and Y. Joshi, "Visualization of droplet departure on a superhydrophobic surface and implications to heat transfer enhancement during dropwise condensation," Appl. Phys. Lett. **97**, 033104 (2010).
[16]H. Kim, S. Yang, S. R. Rao, S. Narayanan, E. A. Kapustin, H. Furukawa, A. S. Umans, O. M. Yaghi, and E. N. Wang, "Water harvesting from air with metal-organic frameworks powered by natural sunlight," Science **356**, 430 (2017).
[17]A. Lee, M.-W. Moon, H. Lim, W.-D. Kim, and H.-Y. Kim, "Water harvest via dewing," Langmuir **28**, 10183 (2012).
[18]F. Liu, G. Ghigliotti, J. J. Feng, and C.-H. Chen, "Self-propelled jumping upon drop coalescence on Leidenfrost surfaces," J. Fluid Mech. **752**, 22 (2014).
[19]F.-C. Wang, F. Yang, and Y.-P. Zhao, "Size effect on the coalescence-induced self-propelled droplet," Appl. Phys. Lett. **98**, 053112 (2011).
[20]F. Liu, G. Ghigliotti, J. J. Feng, and C.-H. Chen, "Numerical simulations of self-propelled jumping upon drop coalescence on non-wetting surfaces," J. Fluid Mech. **752**, 39 (2014).
[21]Y. Wang and P. Ming, "Dynamic and energy analysis of coalescence-induced self-propelled jumping of binary unequal-sized droplets," Phys. Fluids **31**, 122108 (2019).
[22]X. Chen, J. Lu, and G. Tryggvason, "Numerical simulation of self-propelled non-equal sized droplets," Phys. Fluids **31**, 052107 (2019).
[23]Z. Yuan, X. Wu, and Z. Hu, "Rotation of a rebounding-coalescing droplet on a superhydrophobic surface," Phys. Fluids **31**, 062109 (2019).
[24]B. Bhushan and Y. C. Jung, "Natural and biomimetic artificial surfaces for superhydrophobicity, self-cleaning, low adhesion, and drag reduction," Prog. Mater. Sci. **56**, 1 (2011).
[25]Z. Burton and B. Bhushan, "Hydrophobicity, adhesion, and friction properties of nanopatterned polymers and scale dependence for micro- and nanoelectromechanical systems," Nano Lett. **5**, 1607 (2005).
[26]L. Gao and T. J. McCarthy, "The 'lotus effect' explained: Two reasons why two length scales of topography are important," Langmuir **22**, 2966 (2006).
[27]A. Giacomello, M. Chinappi, S. Meloni, and C. M. Casciola, "Metastable wetting on superhydrophobic surfaces: Continuum and atomistic views of the Cassie-Baxter–Wenzel transition," Phys. Rev. Lett. **109**, 226102 (2012).
[28]D. Wu, S.-Z. Wu, Q.-D. Chen, Y.-L. Zhang, J. Yao, X. Yao, L.-G. Niu, J.-N. Wang, L. Jiang, and H.-B. Sun, "Curvature-driven reversible *in situ* switching between pinned and roll-down superhydrophobic states for water droplet transportation," Adv. Mater. **23**, 545 (2011).
[29]K. Koch, B. Bhushan, Y. C. Jung, and W. Barthlott, "Fabrication of artificial lotus leaves and significance of hierarchical structure for superhydrophobicity and low adhesion," Soft Matter **5**, 1386 (2009).
[30]Y. Liu, L. Moevius, X. Xu, T. Qian, J. M. Yeomans, and Z. Wang, "Pancake bouncing on superhydrophobic surfaces," Nat. Phys. **10**, 515 (2014).
[31]Z. Liang and P. Keblinski, "Coalescence-induced jumping of nanoscale droplets on super-hydrophobic surfaces," Appl. Phys. Lett. **107**, 143105 (2015).
[32]R. Attarzadeh and A. Dolatabadi, "Coalescence-induced jumping of micro-droplets on heterogeneous superhydrophobic surfaces," Phys. Fluids **29**, 012104 (2017).
[33]Y. Cheng, J. Xu, and Y. Sui, "Numerical investigation of coalescence-induced droplet jumping on superhydrophobic surfaces for efficient dropwise condensation heat transfer," Int. J. Heat Mass Transfer **95**, 506 (2016).
[34]A. Gauthier, S. Symon, C. Clanet, and D. Quéré, "Water impacting on superhydrophobic macrotextures," Nat. Commun. **6**, 8001 (2015).
[35]M. Baggio and B. Weigand, "Numerical simulation of a drop impact on a superhydrophobic surface with a wire," Phys. Fluids **31**, 112107 (2019).
[36]C. Hao, J. Li, Y. Liu, X. Zhou, Y. Liu, R. Liu, L. Che, W. Zhou, D. Sun, and L. Li, "Superhydrophobic-like tunable droplet bouncing on slippery liquid interfaces," Nat. Commun. **6**, 7986 (2015).
[37]Y. Liu, M. Andrew, J. Li, J. M. Yeomans, and Z. Wang, "Symmetry breaking in drop bouncing on curved surfaces," Nat. Commun. **6**, 10034 (2015).
[38]J. De Ruiter, R. Lagraauw, D. Van Den Ende, and F. Mugele, "Wettability-independent bouncing on flat surfaces mediated by thin air films," Nat. Phys. **11**, 48 (2015).
[39]J. M. Kolinski, L. Mahadevan, and S. M. Rubinstein, "Drops can bounce from perfectly hydrophilic surfaces," Europhys. Lett. **108**, 24001 (2014).
[40]D. Richard, C. Clanet, and D. Quéré, "Surface phenomena: Contact time of a bouncing drop," Nature **417**, 811 (2002).
[41]K. Zhang, F. Liu, A. J. Williams, X. Qu, J. J. Feng, and C.-H. Chen, "Self-propelled droplet removal from hydrophobic fiber-based coalescers," Phys. Rev. Lett. **115**, 074502 (2015).
[42]Y. Nam, H. Kim, and S. Shin, "Energy and hydrodynamic analyses of coalescence-induced jumping droplets," Appl. Phys. Lett. **103**, 161601 (2013).
[43]Y. Chen and Y. Lian, "Numerical investigation of coalescence-induced self-propelled behavior of droplets on non-wetting surfaces," Phys. Fluids **30**, 112102 (2018).
[44]R. Enright, N. Miljkovic, J. Sprittles, K. Nolan, R. Mitchell, and E. N. Wang, "How coalescing droplets jump," ACS Nano **8**, 10352 (2014).
[45]Y. Guo, Y. Lian, and M. Sussman, "Investigation of drop impact on dry and wet surfaces with consideration of surrounding air," Phys. Fluids **28**, 073303 (2016).
[46]M. Jemison, E. Loch, M. Sussman, M. Shashkov, M. Arienti, M. Ohta, and Y. Wang, "A coupled level set-moment of fluid method for incompressible two-phase flows," J. Sci. Comput. **54**, 454 (2013).
[47]G. Li, Y. Lian, Y. Guo, M. Jemison, M. Sussman, T. Helms, and M. Arienti, "Incompressible multiphase flow and encapsulation simulations using the moment-of-fluid method," Int. J. Numer. Methods Fluids **79**, 456 (2015).
[48]H. T. Ahn and M. Shashkov, "Multi-material interface reconstruction on generalized polyhedral meshes," J. Comput. Phys. **226**, 2096 (2007).
[49]H. T. Ahn and M. Shashkov, "Adaptive moment-of-fluid method," J. Comput. Phys. **228**, 2792 (2009).
[50]V. Dyadechko and M. Shashkov, "Moment-of-fluid interface reconstruction," Los Alamos Report LA-UR-05-7571, 2005.
[51]V. Dyadechko and M. Shashkov, "Reconstruction of multi-material interfaces from moment data," J. Comput. Phys. **227**, 5361 (2008).
[52]H. T. Ahn, M. Shashkov, and M. A. Christon, "The moment-of-fluid method in action," Comm. Numer. Meth. Eng. **25**(10), 1009–1018 (2009).
[53]T.-S. Jiang, O. H. Soo-Gun, and J. C. Slattery, "Correlation for dynamic contact angle," J. Colloid Interface Sci. **69**, 74 (1979).
[54]R. L. Hoffman, "A study of the advancing interface. I. Interface shape in liquid-gas systems," J. Colloid Interface Sci. **50**, 228 (1975).
[55]K. Yokoi, D. Vadillo, J. Hinch, and I. Hutchings, "Numerical studies of the influence of the dynamic contact angle on a droplet impacting on a dry surface," Phys. Fluids **21**, 072102 (2009).
[56]L. Mishchenko, B. Hatton, V. Bahadur, J. A. Taylor, T. Krupenkin, and J. Aizenberg, "Design of ice-free nanostructured surfaces based on repulsion of impacting water droplets," ACS Nano **4**, 7699 (2010).
[57]H. A. Stone, "Ice-phobic surfaces that are wet," ACS Nano **6**, 6536 (2012).
[58]N. Savage, "Synthetic coatings: Super surfaces," Nature **519**, S7 (2015).
[59]T. Gilet and L. Bourouiba, "Rain-induced ejection of pathogens from leaves: Revisiting the hypothesis of splash-on-film using high-speed visualization," Integr. Comp. Biol. **54**, 974 (2014).
[60]K. Graf and M. Kappl, *Physics and Chemistry of Interfaces* (John Wiley & Sons, 2006).